Sample Development for Small Angle Scattering and Neutron Interferometry

KAITLYN ESNEAULT

CAITLYN WOLF -- MENTOR

KATIE WEIGANDT -- MENTOR

NIST SURF PROGRAM 2023

Small Angle Scattering (SAS)

- Statistical **characterization** of materials
  - Reveals interatomic detail smaller than wavelength of visible light
  - Works at length scales of **1nm – 10µm**

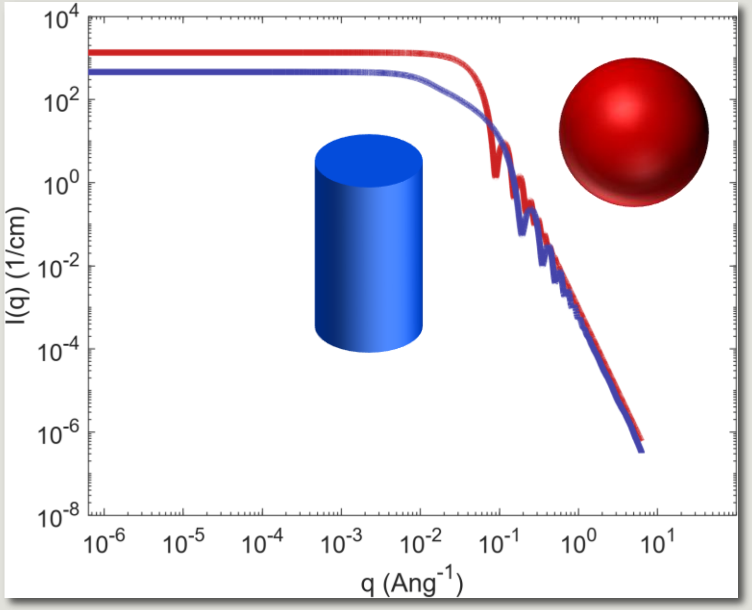

$$I(Q) = \phi \Delta\rho^2 P(Q) S(Q)$$

- Small Angle X-Ray Scattering (SAXS)
  - Scattered by **electrons** in material
  - Good for heavy elements with many electrons

- Small Angle Neutron Scattering (SANS)
  - Scattered by **nuclei** in material
  - Much better penetration, but weaker scattering effect

$$\boxed{Q = \frac{4\pi}{\lambda}\sin\left(\frac{\theta}{2}\right)}$$

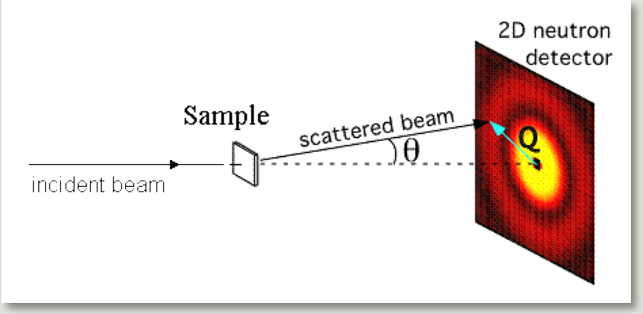

https://www.nist.gov/image/scatteringgif-0

- **Difficult to use for heterogenous samples**

Neutron Interferometry & INFER

- Characterize materials at **multiple length scales** simultaneously
  - Dark field interferometry: 1nm-10μm (same as SAS)
  - Direct imaging: 50μm-100μm
- SAS information for more complex (**heterogenous** or **hierarchical**) materials
- Data is **related to SAS data** by a Hankel transform

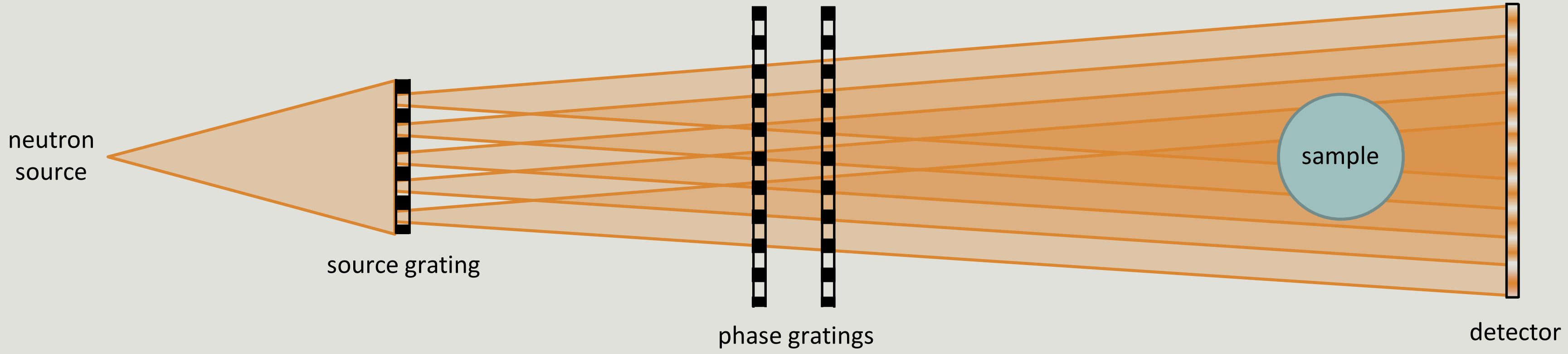

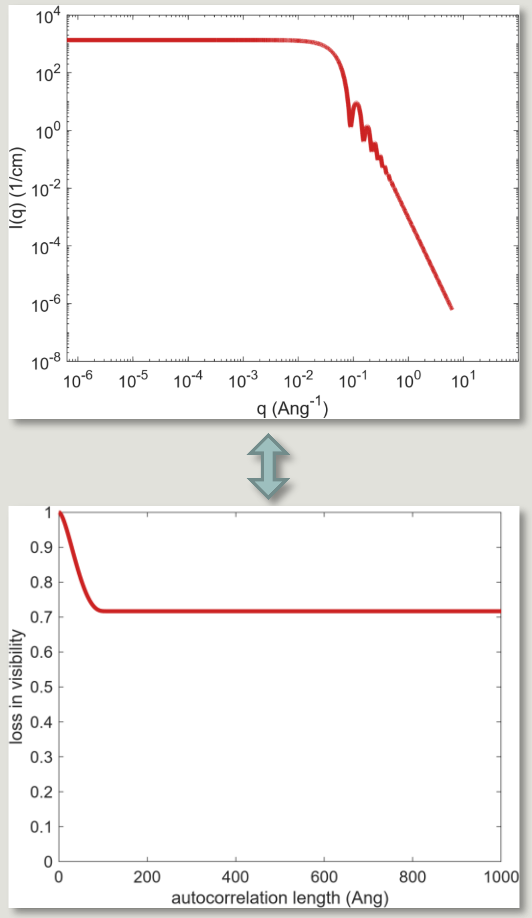

Sample System

- Self-assembling **S**odium **D**odecyl **S**ulfate / **β-C**yclo**d**extrin complex (SDS@2β-CD)
- **Concentration-dependent** phase behavior

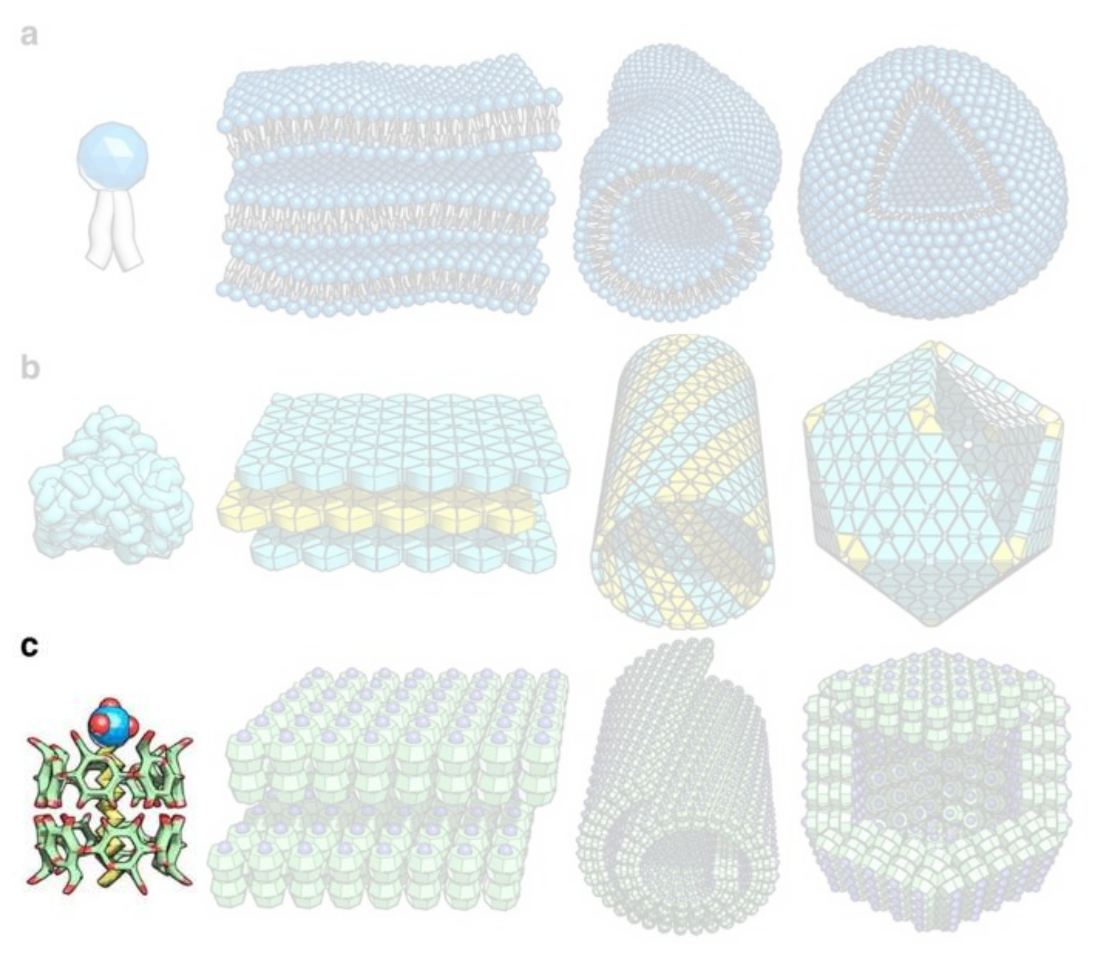

Figure 1. Stylized view of the lipid-like and protein-like self-assembly. Yang, S., Yan, Y., Huang, J. *et al.* Giant capsids from lattice self-assembly of cyclodextrin complexes. *Nat Commun* **8**, 15856 (2017). https://doi.org/10.1038/ncomms15856

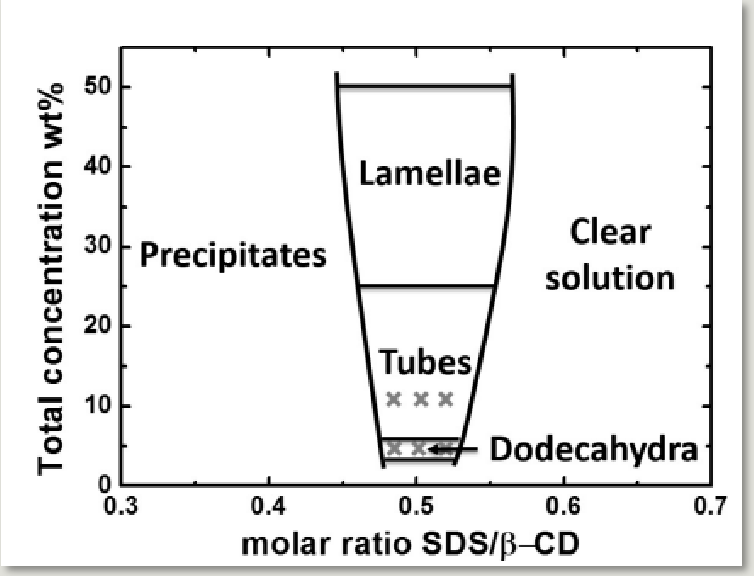

Supplementary Figure 1. The general phase diagram of the SDS/β-CD aqueous solution at room temperature. Yang, S., Yan, Y., Huang, J. *et al.* Giant capsids from lattice self-assembly of cyclodextrin complexes. *Nat Commun* **8**, 15856 (2017). https://doi.org/10.1038/ncomms15856

My Objectives

1. Develop a more comprehensive **phase space** for the SDS@2β-CD system using SAS characterization techniques
2. Facilitate the system's use in **testing the accuracy** of a novel far field interferometer

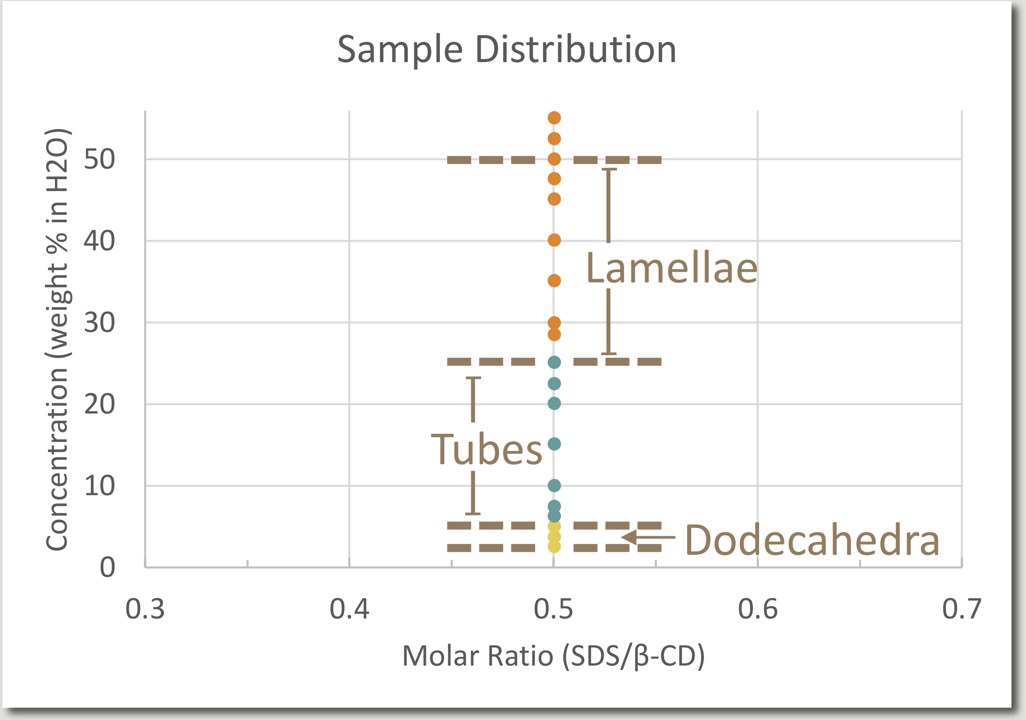

Preliminary Samples

- **Recreate** literature findings
- Dynamic Light Scattering (DLS)
  - Look for trends in particle radii
- Small Angle X-Ray Scattering (SAXS)
  - Get structural information from data fitting

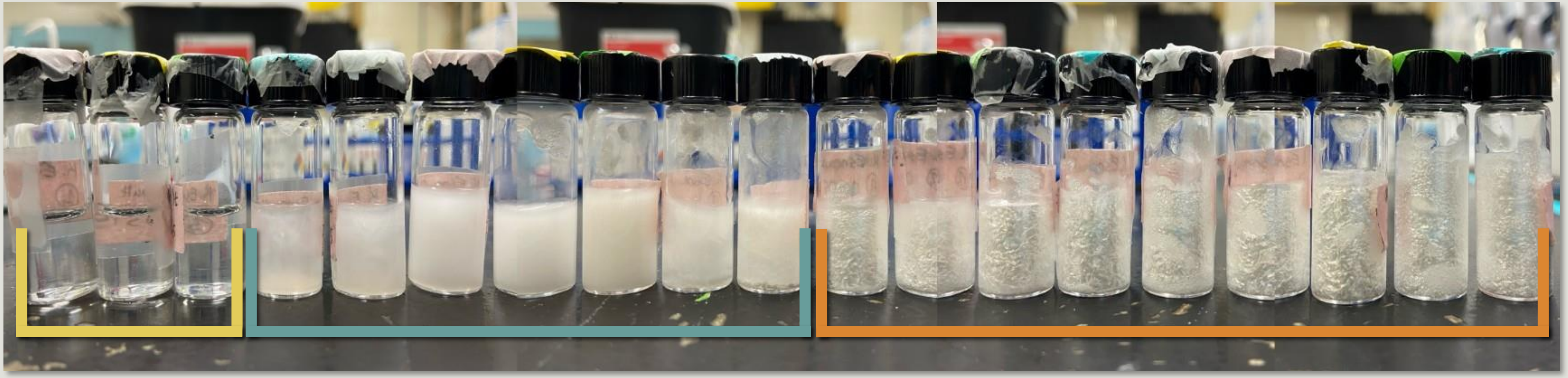

SAXS results

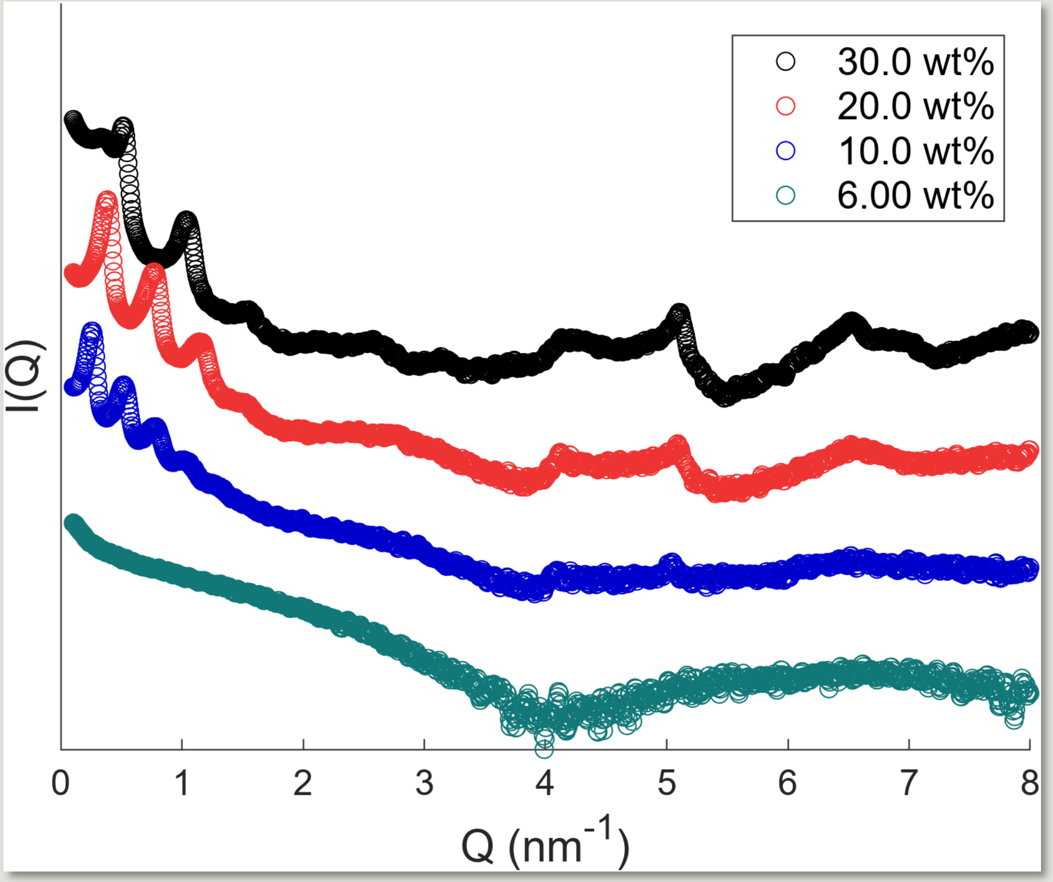

Graphs are artificially spaced out along y-axis for clarity

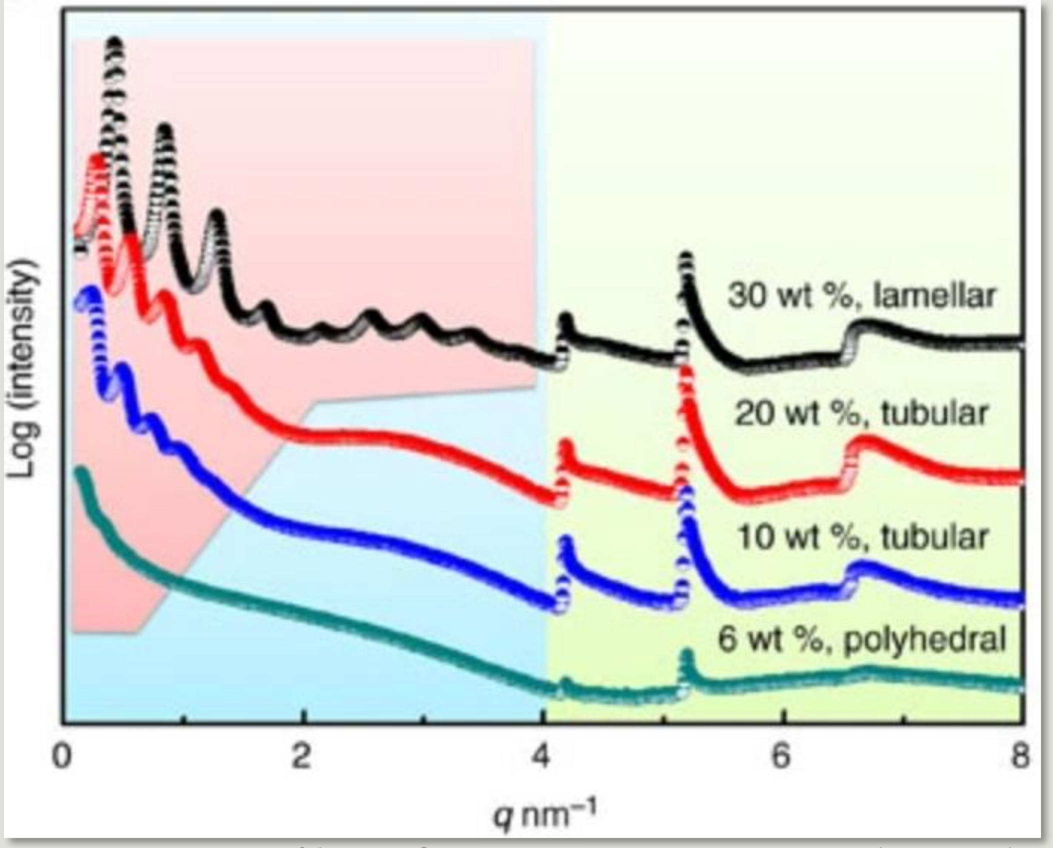

Figure 4a. X-ray scattering of the SDS@2β-CD structures. Yang, S., Yan, Y., Huang, J. *et al.* Giant capsids from lattice self-assembly of cyclodextrin complexes. *Nat Commun* **8**, 15856 (2017). https://doi.org/10.1038/ncomms15856

SAXS results

$$\frac{2\pi}{4.1} \approx 1.52$$

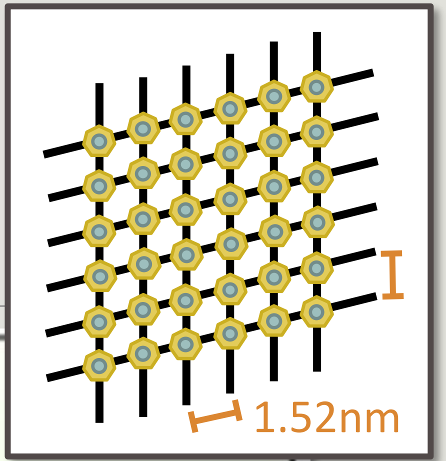

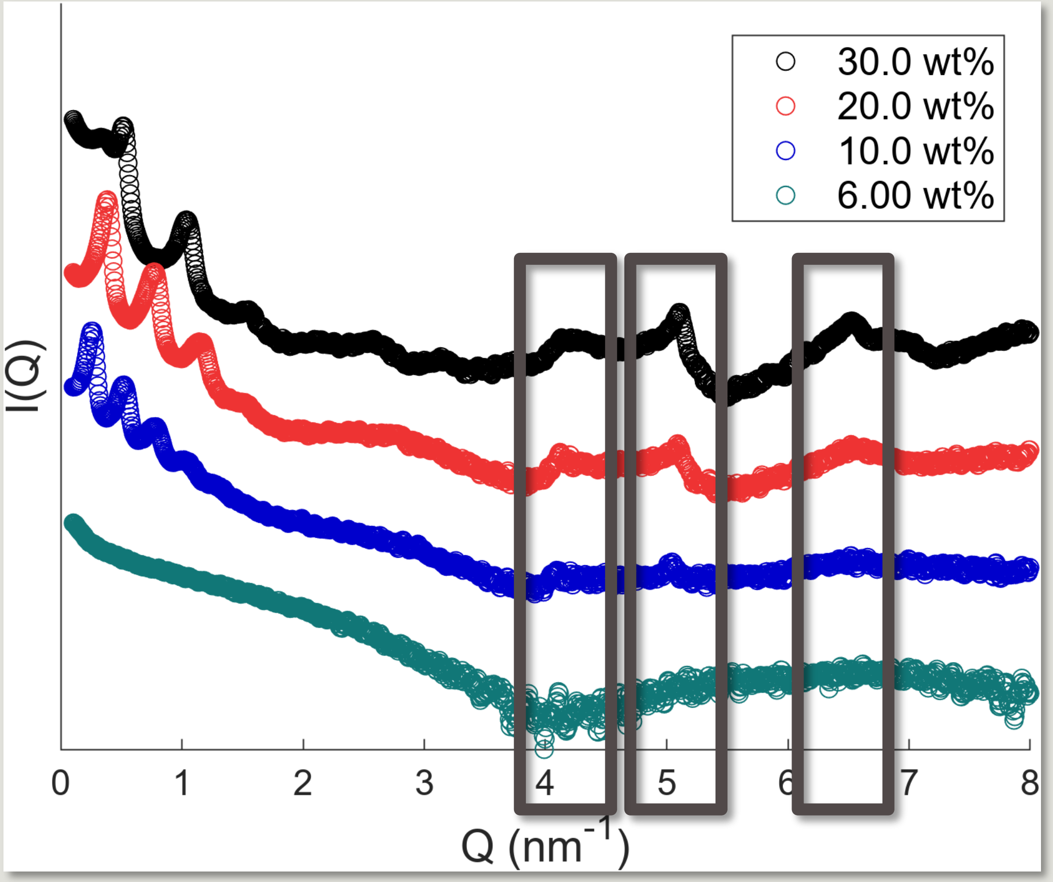

Graphs are artificially spaced out along y-axis for clarity

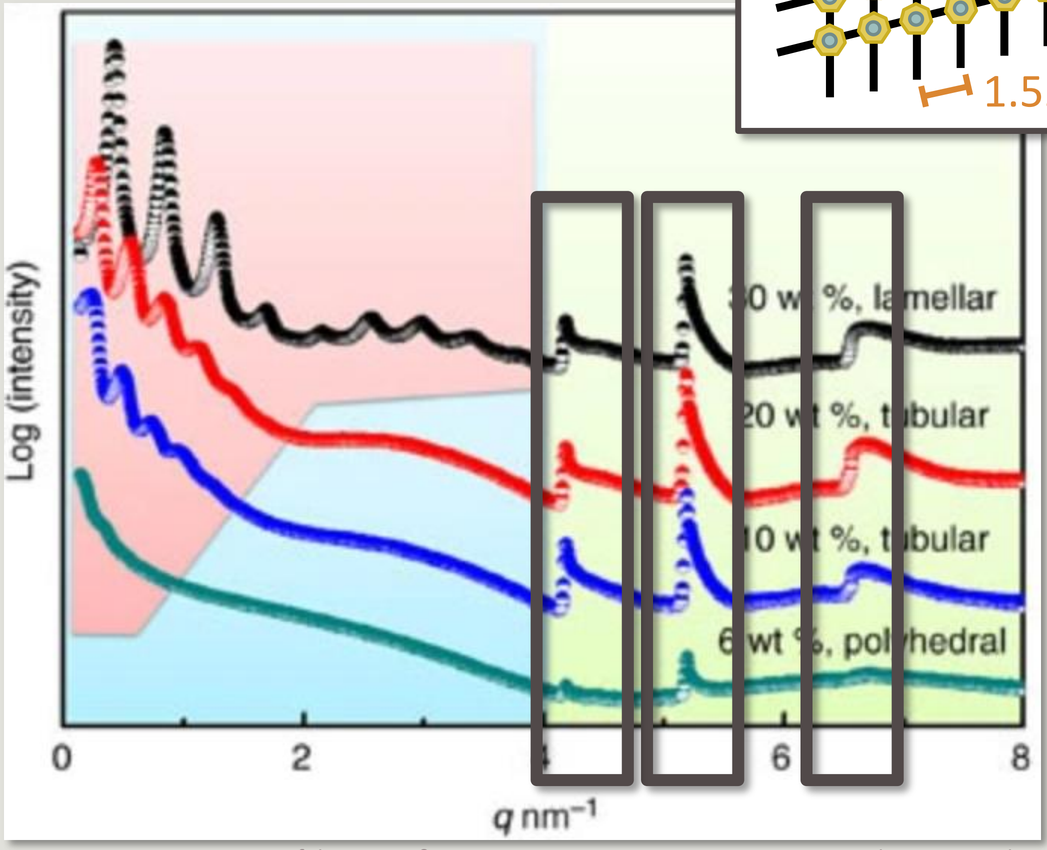

Figure 4a. X-ray scattering of the SDS@2β-CD structures. Yang, S., Yan, Y., Huang, J. *et al.* Giant capsids from lattice self-assembly of cyclodextrin complexes. *Nat Commun* **8**, 15856 (2017). https://doi.org/10.1038/ncomms15856

SAXS results

$$\frac{2\pi}{1.8} \approx 3.5$$

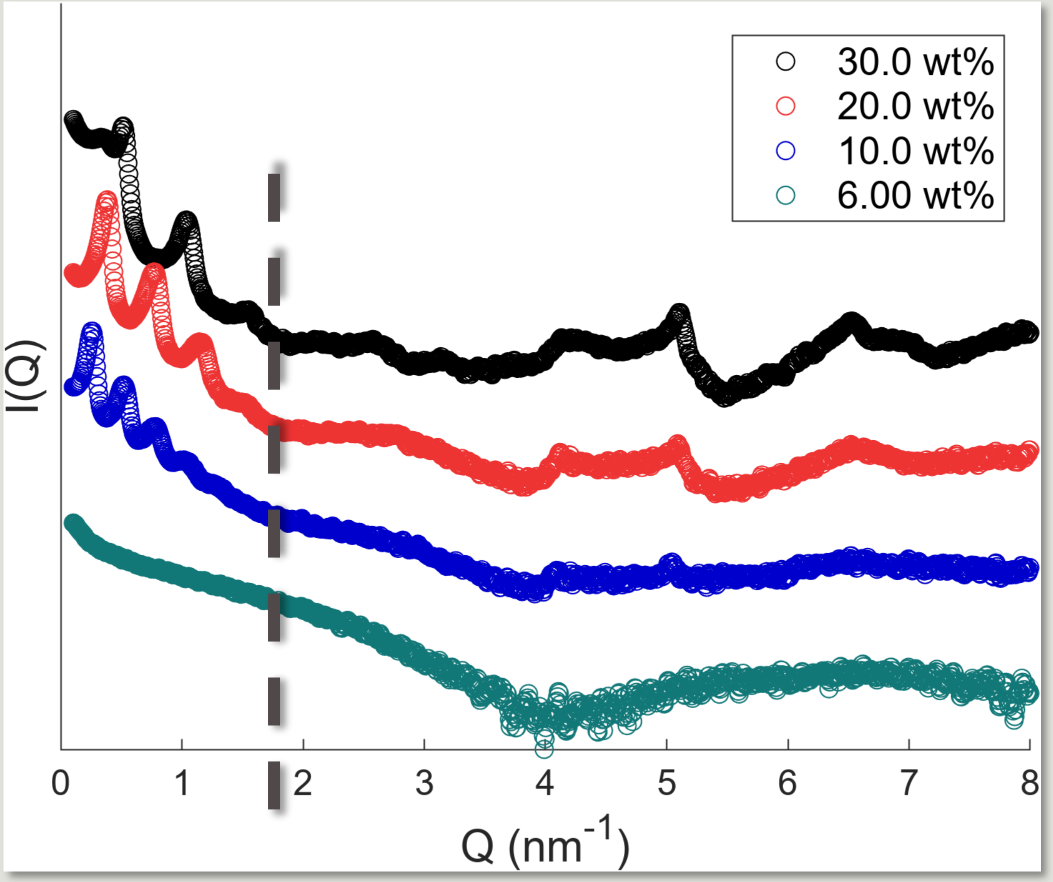

Graphs are artificially spaced out along y-axis for clarity

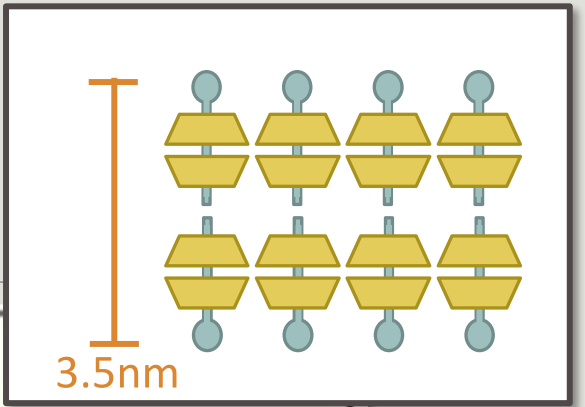

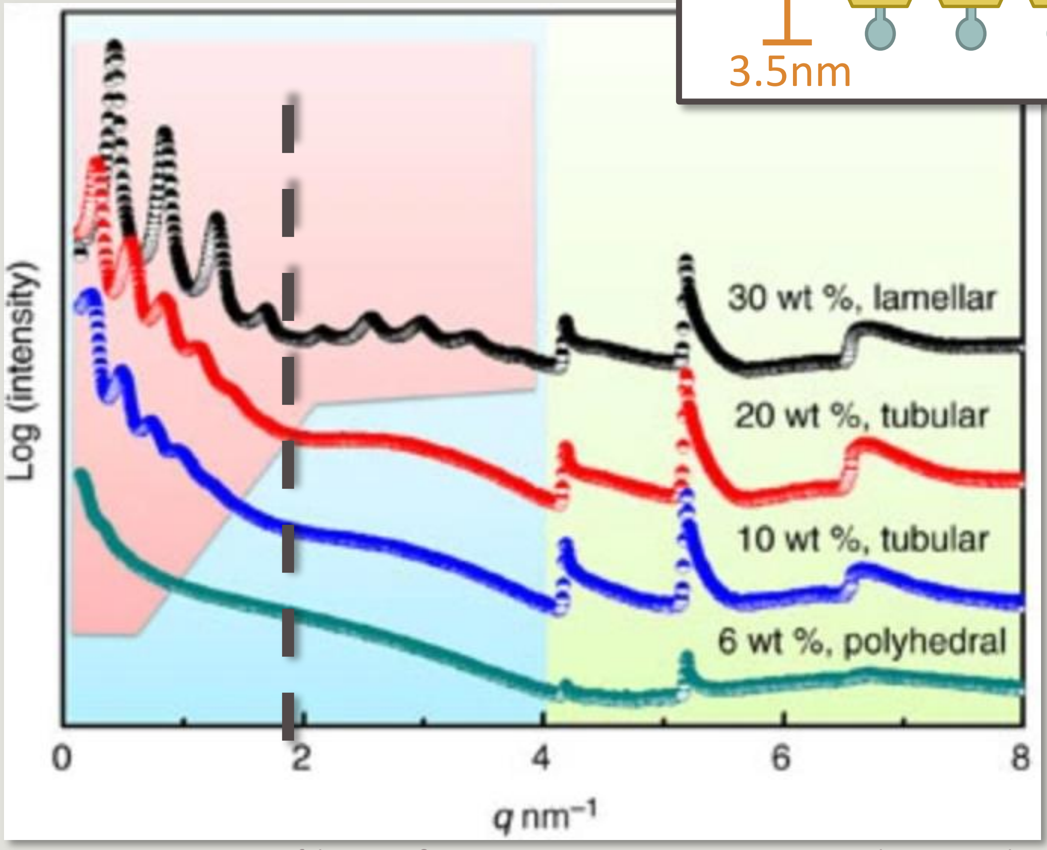

Figure 4a. X-ray scattering of the SDS@2β-CD structures. Yang, S., Yan, Y., Huang, J. *et al.* Giant capsids from lattice self-assembly of cyclodextrin complexes. *Nat Commun* **8**, 15856 (2017). https://doi.org/10.1038/ncomms15856

SAXS results

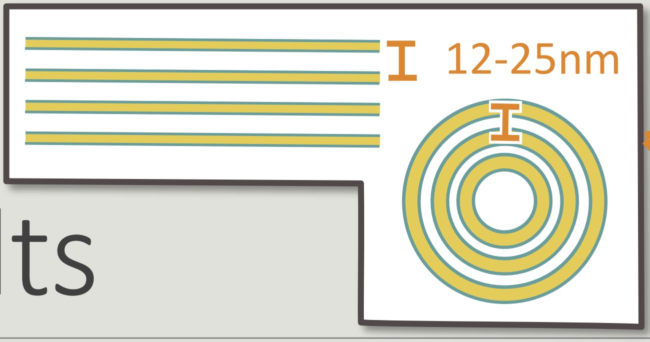

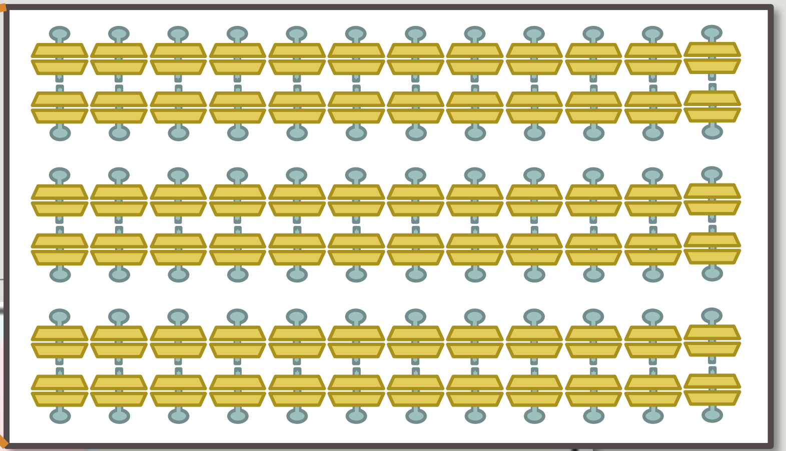

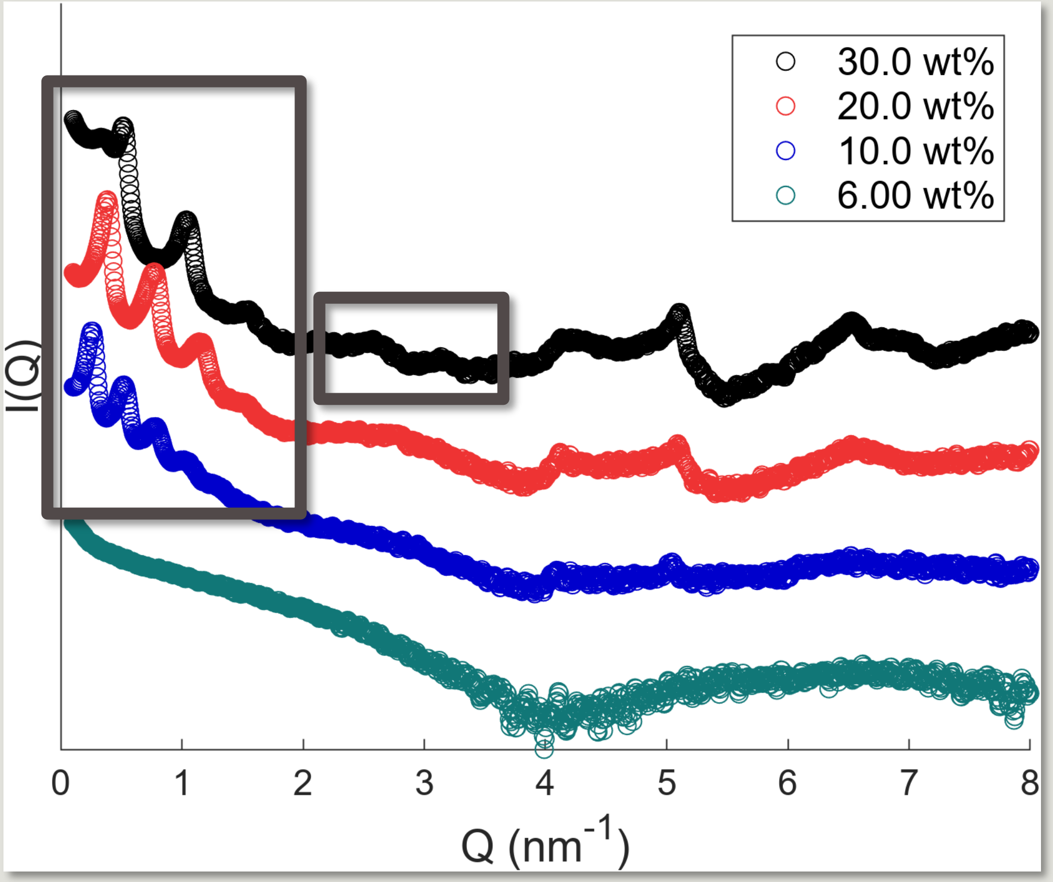

Graphs are artificially spaced out along y-axis for clarity

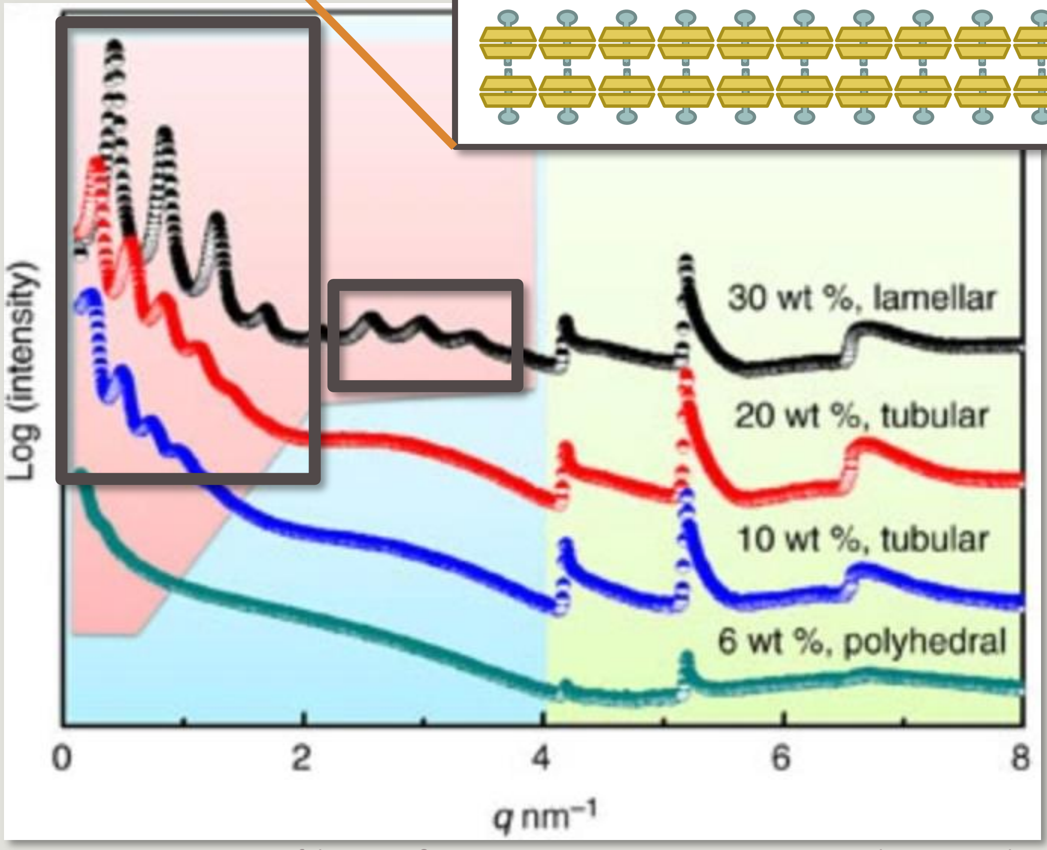

Figure 4a. X-ray scattering of the SDS@2β-CD structures. Yang, S., Yan, Y., Huang, J. *et al.* Giant capsids from lattice self-assembly of cyclodextrin complexes. *Nat Commun* **8**, 15856 (2017). https://doi.org/10.1038/ncomms15856

SAXS results

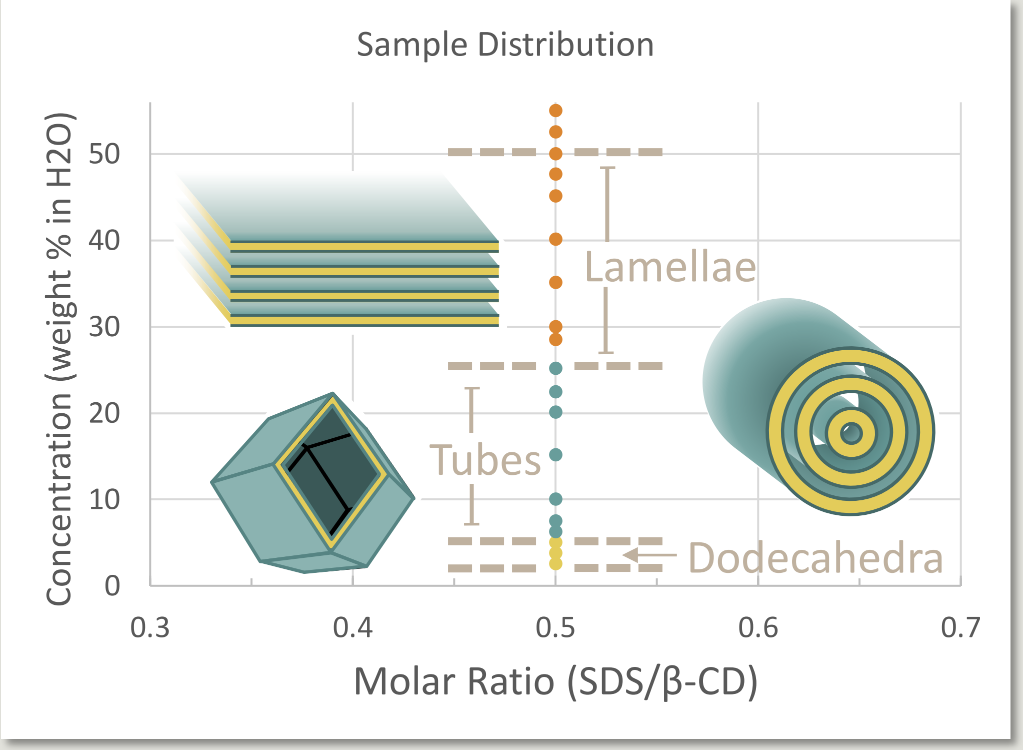

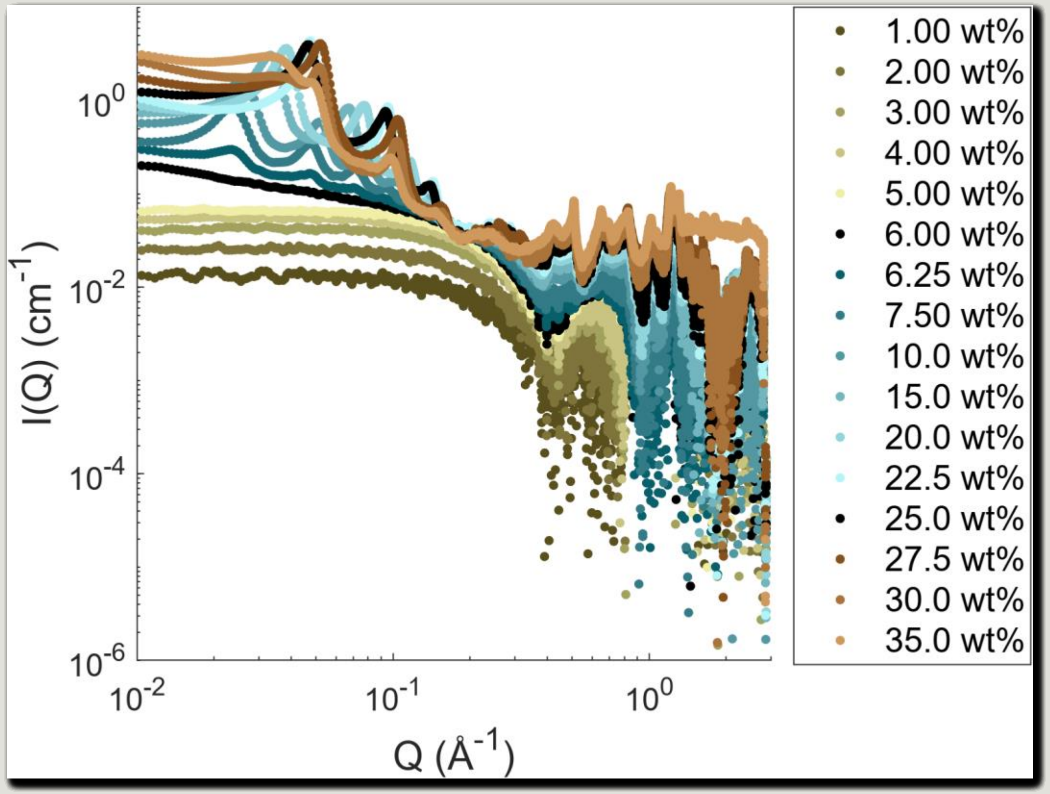

Data Fitting

- SASView (www.sasview.org)
  - *lamellar_stack_paracrystal* form factor
    - Incorporates **bilayer form factor** and a term to account for interference caused by having **lamellar stacks of bilayers**
- Key parameters:
  - **thickness** – thickness of layers

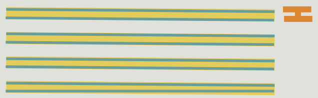

  - **Nlayers** – number of layers

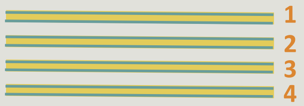

  - **d_spacing** – spacing between layers

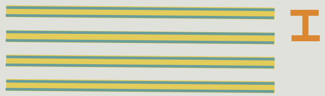

$$I(Q) = \phi \Delta\rho^2 \boldsymbol{P}(\boldsymbol{Q}) S(Q)$$

- Used for **lamellar** phase and **microtube** phase

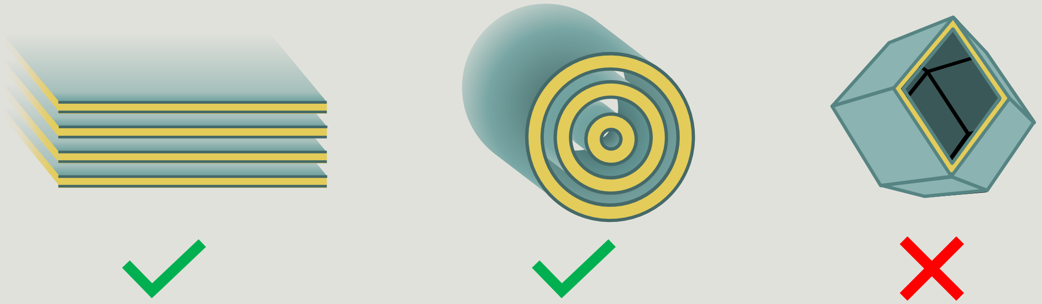

Data Fitting

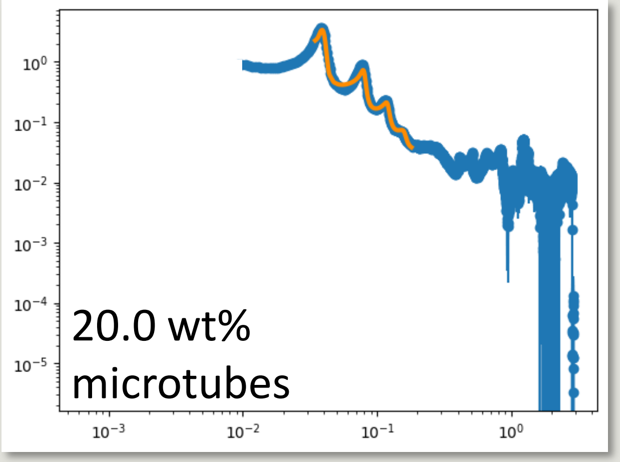

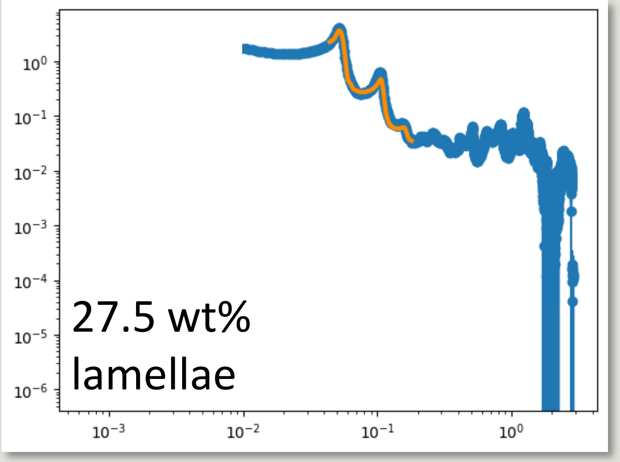

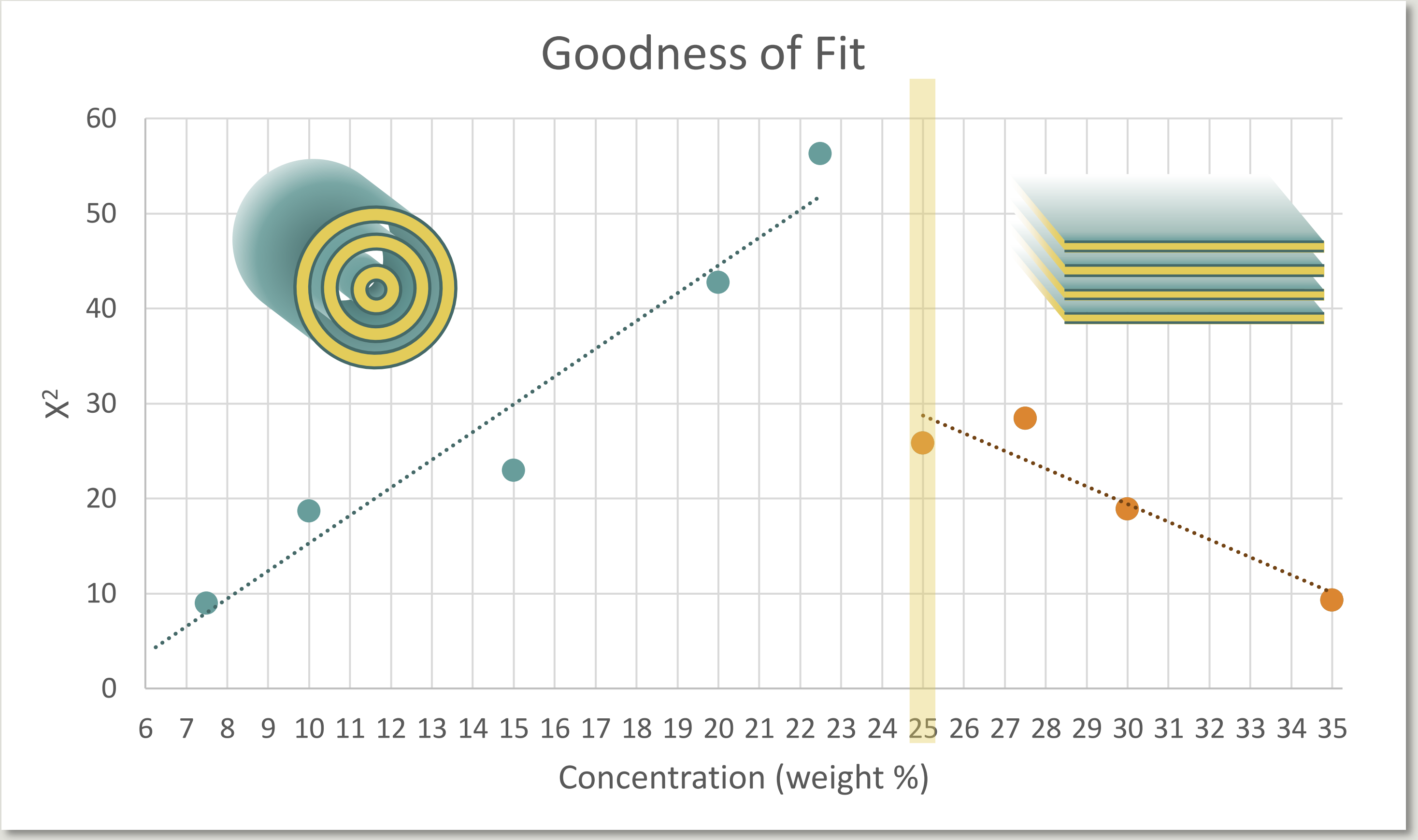

Data Fitting

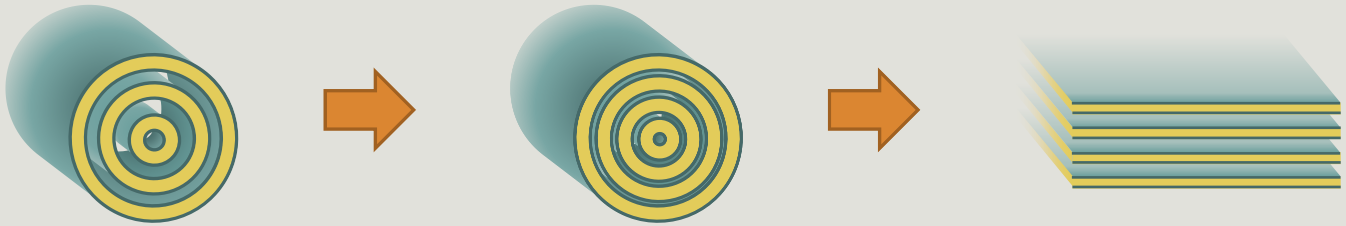

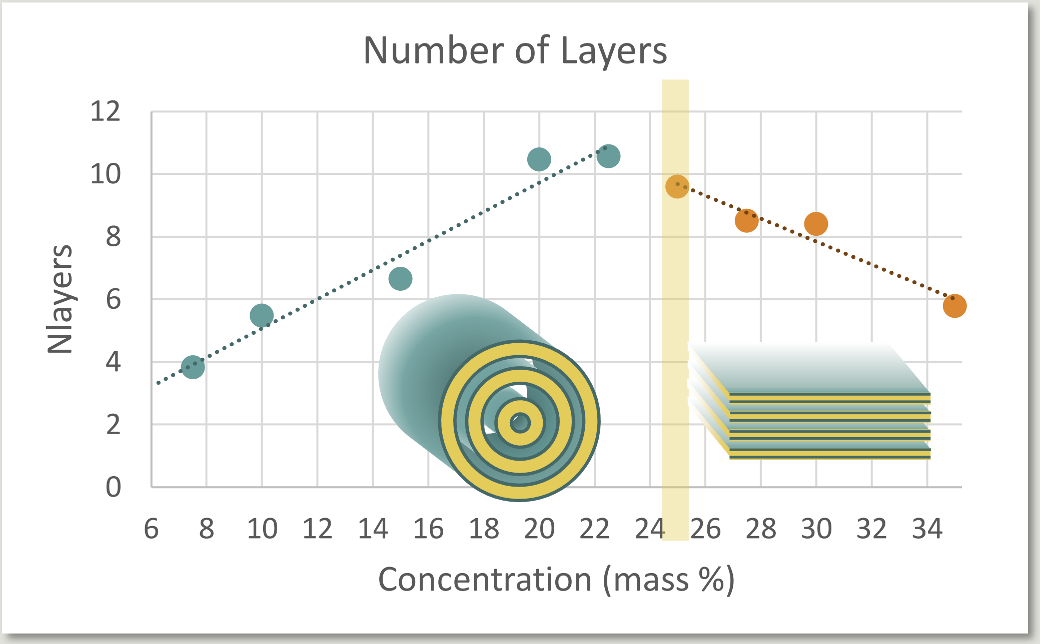

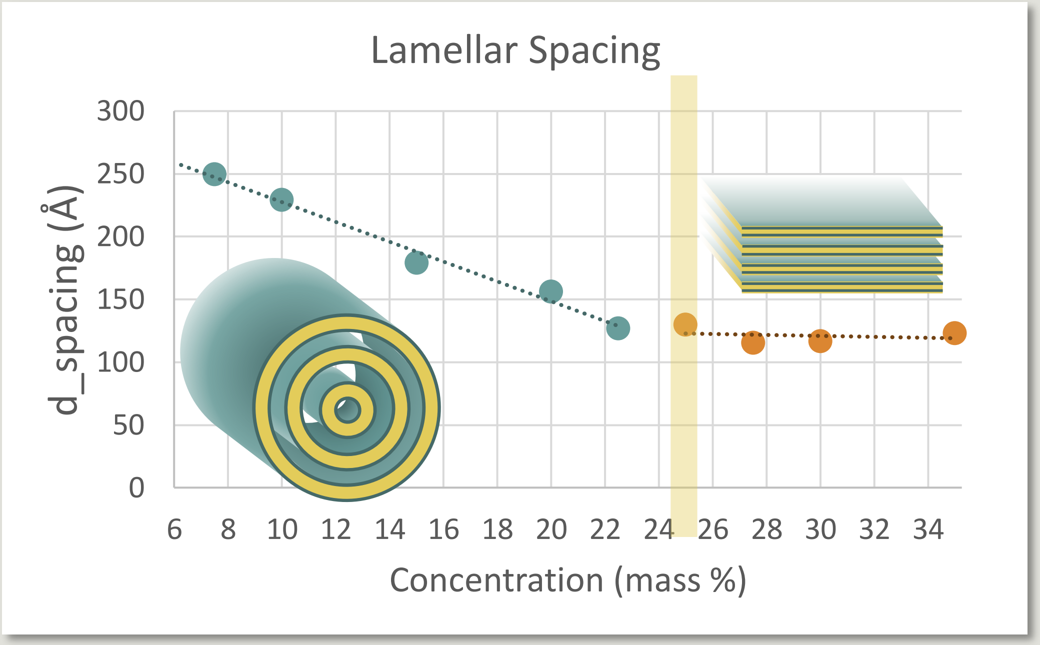

*** Error bars are too small to be visible on these graphs ***

SANS Data

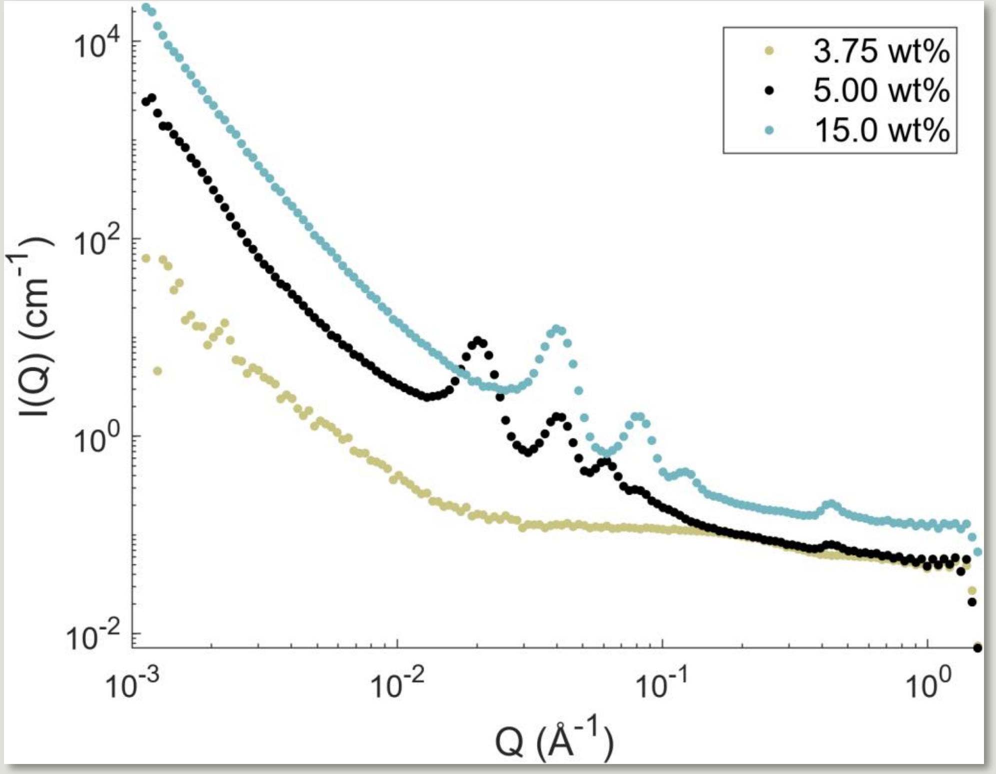

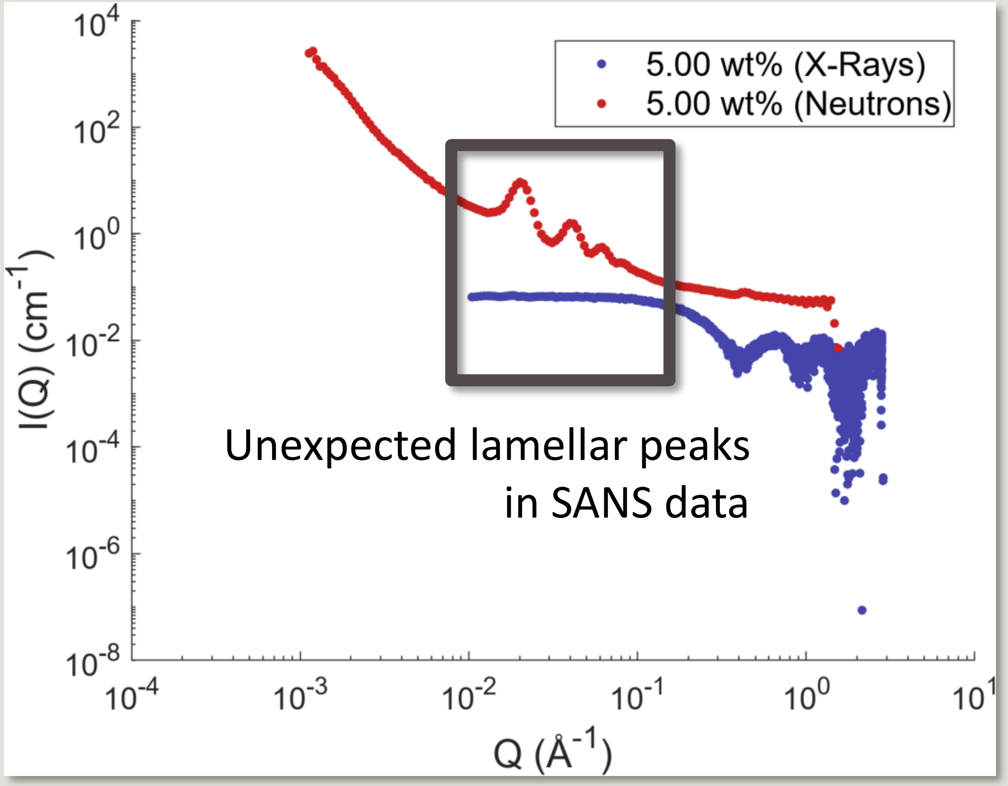

SANS data was collected by Katie Weigandt and Kelsi Rehmann at the Australian Nuclear Science and Technology Organisation (ANSTO) on the Bilby beamline

SANS Data

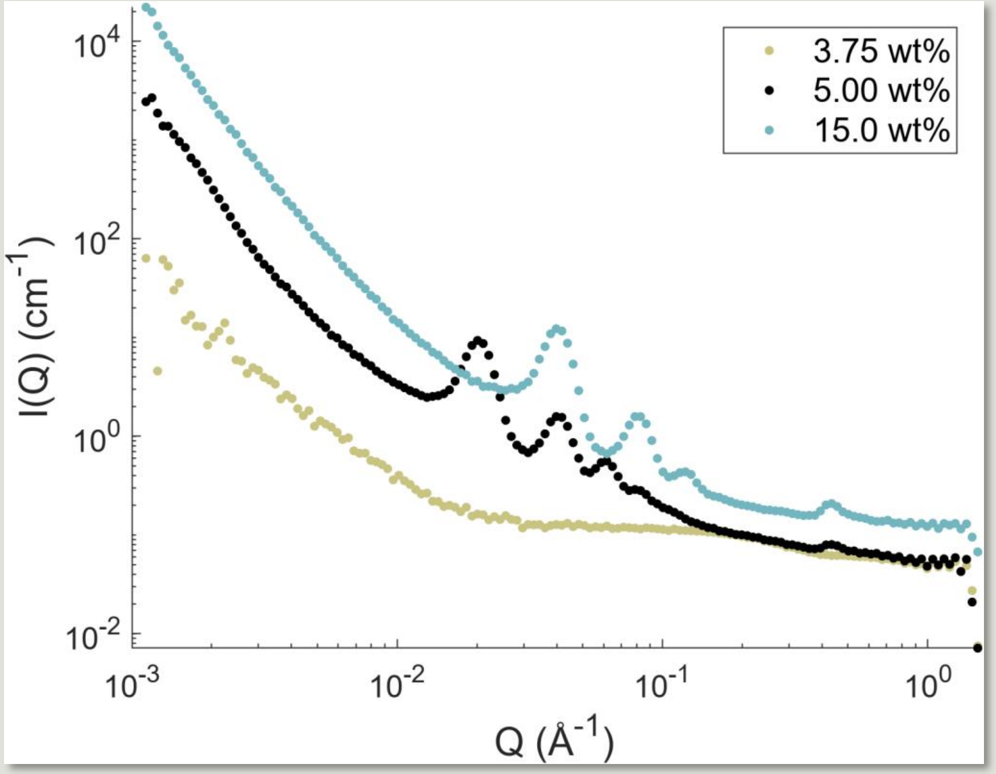

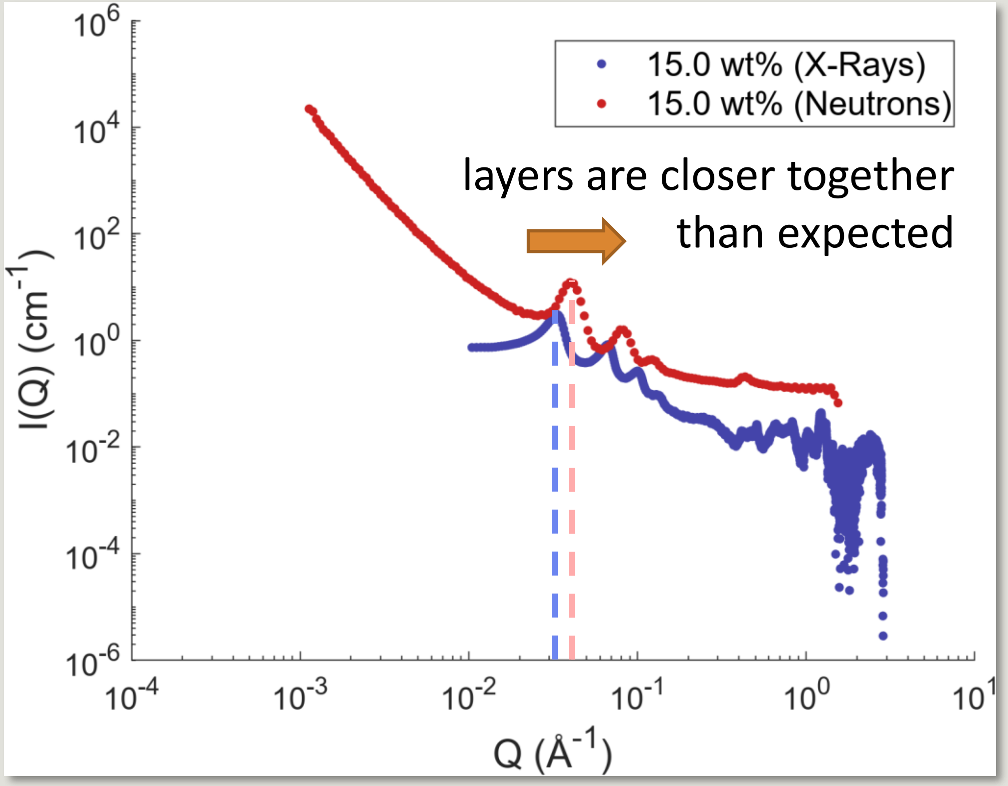

- Samples prepared in **D2O** rather than H2O

SANS data was collected by Katie Weigandt and Kelsi Rehmann at the Australian Nuclear Science and Technology Organisation (ANSTO) on the Bilby beamline

Transformation to Dark Field Intensity

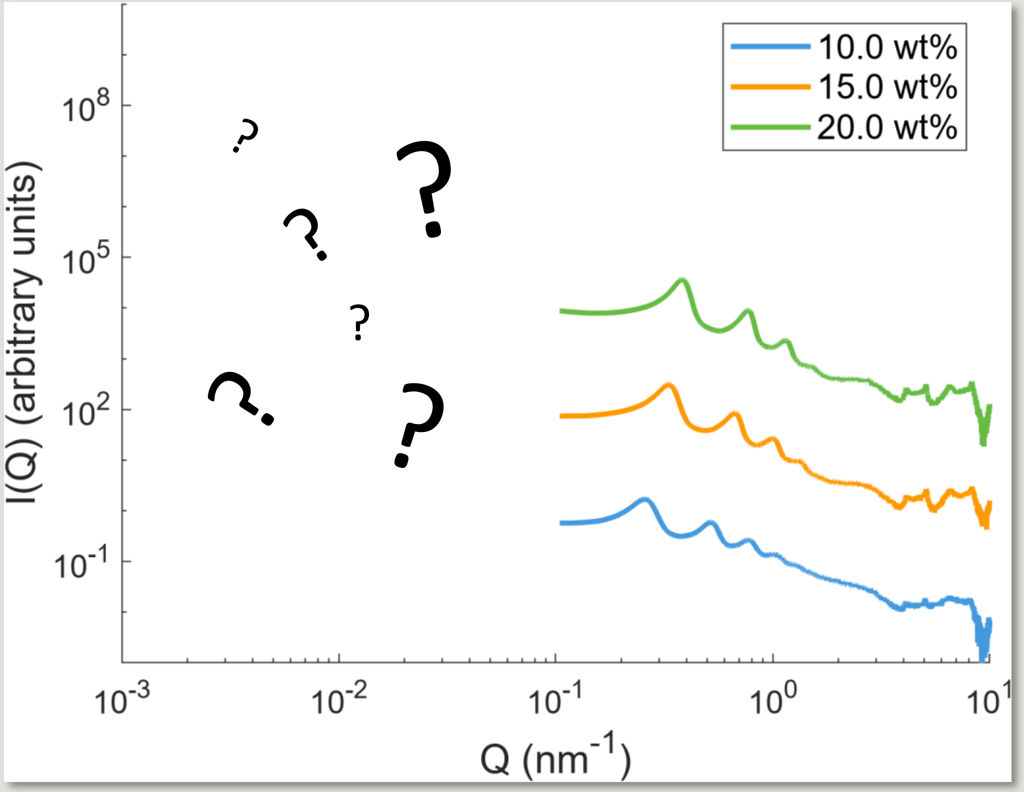

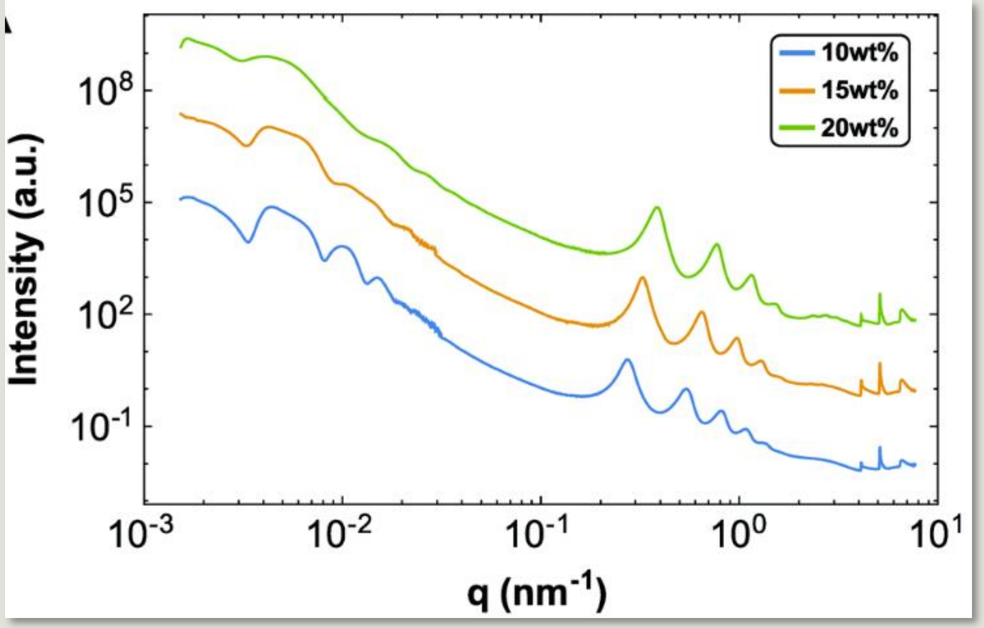

Figure 4a. The response of the thermo-reversible microtubes to variations in concentration. Ouhajji, Samia, *et al*. In Situ Observation of Self-Assembly of Sugars and Surfactants from Nanometres to Microns. *Soft Matter*, vol. 13, no. 13, Mar. 2017, pp. 2421–25. *pubs.rsc.org*, https://doi.org/10.1039/C7SM00109F.

Transformation to Dark Field Intensity

- Add *hollow_cylinder* form factor to **approximate low-Q data** from literature values

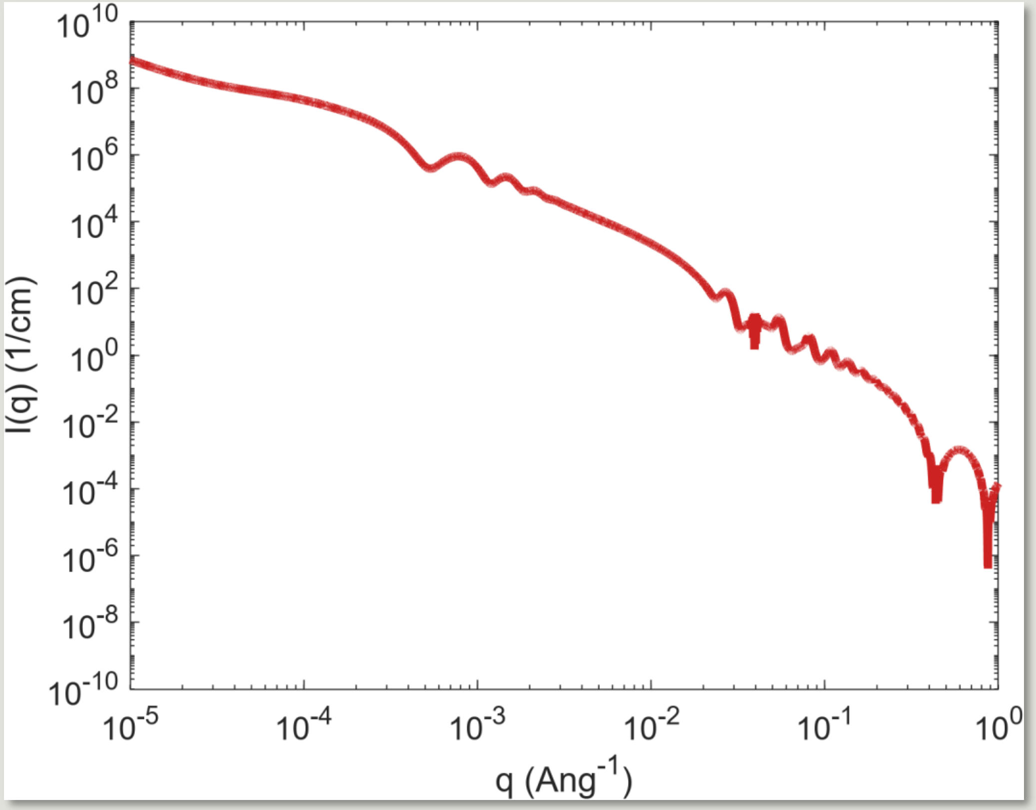

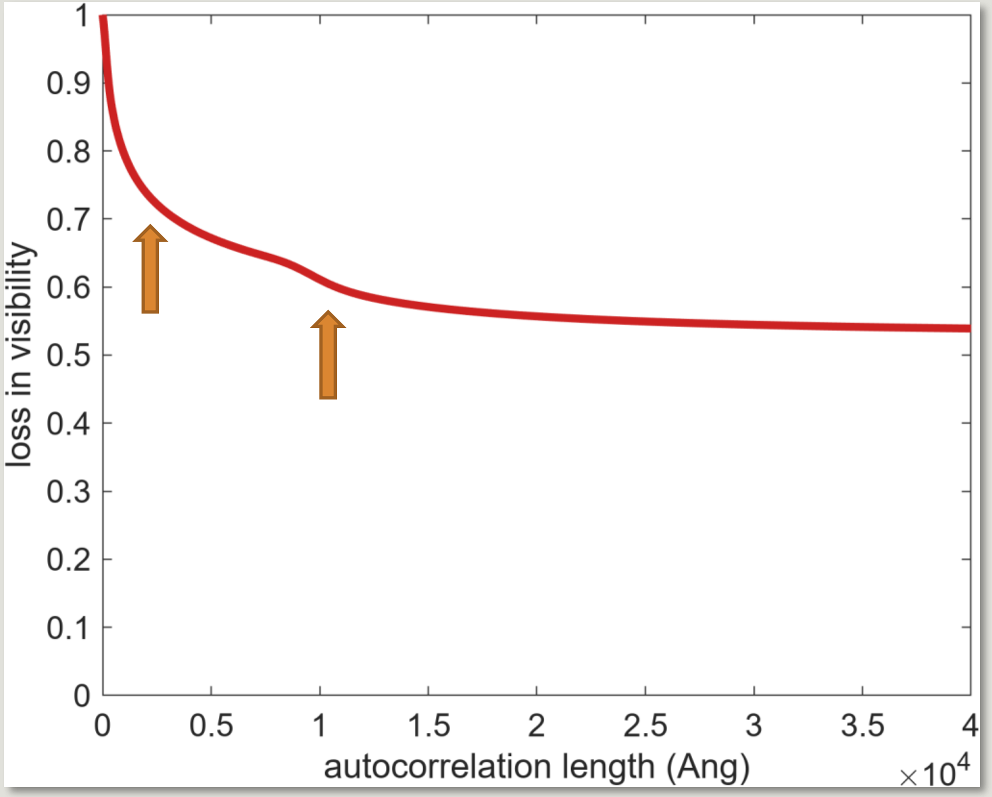

Conclusions & Future Research

- This system is a **good candidate** for validating data from the new interferometer
- Areas for further study:
  - Other **cyclodextrins**
  - Effect of **D2O**
  - More powerful **SAS** instrument for lower Q study
  - Better **models** for dodecahedral and microtube phases

References

1. Landman, J. *et al.* Inward growth by nucleation: Multiscale self-assembly of ordered membranes. *Sci. Adv.* **4**, eaat1817 (2018). https://doi.org/10.1126/sciadv.aat1817
2. Strobl, M. General solution for quantitative dark-field contrast imaging with grating interferometers. *Sci Rep* **4**, 7243 (2014). https://doi.org/10.1038/srep07243
3. Wolf, C. M. *et al.* Blend Morphology in Polythiophene–Polystyrene Composites from Neutron and X-ray Scattering. *Macromolecules* **54** (6), 2960 (2021). https://doi.org/10.1021/acs.macromol.0c02512
4. Yang, S., Yan, Y., Huang, J. *et al.* Giant capsids from lattice self-assembly of cyclodextrin complexes. *Nat Commun* **8**, 15856 (2017). https://doi.org/10.1038/ncomms1585

This work benefited from the use of the SasView application, originally developed under NSF award DMR-0520547. SasView also contains code developed with funding from the European Union's Horizon 2020 research and innovation programme under the SINE2020 project, grant agreement No 654000.

Supplemental Slides

lamellar_stack_paracrystal thickness parameter

- Bilayer thickness should be constant
- Further evidence this model may not be the best fit for the microtube phase
- Perhaps an artifact from the curvature of the tubes
- Note the error bar on the 7.5 wt% sample

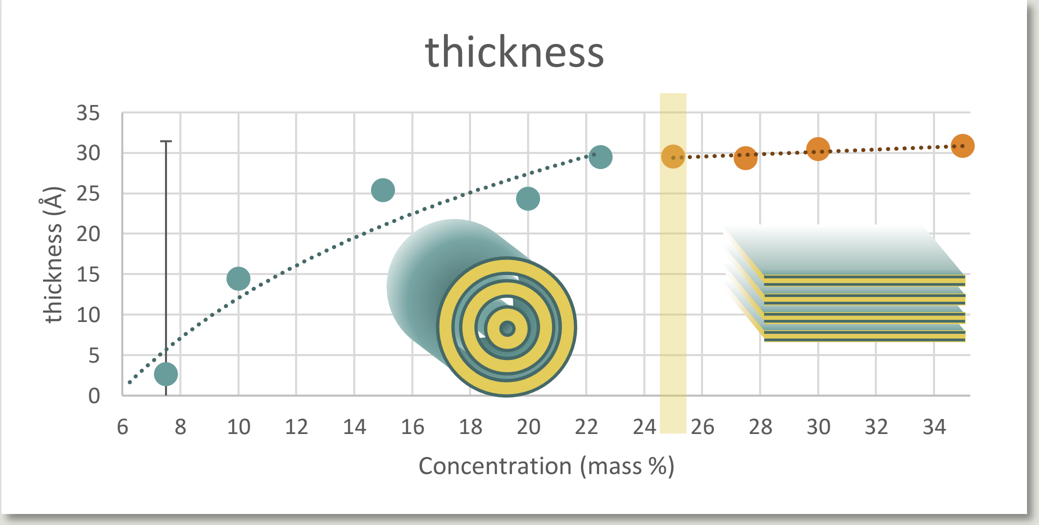

30 wt% Sample SANS Data

- Suspected issues loading sample – lamellar peaks absent

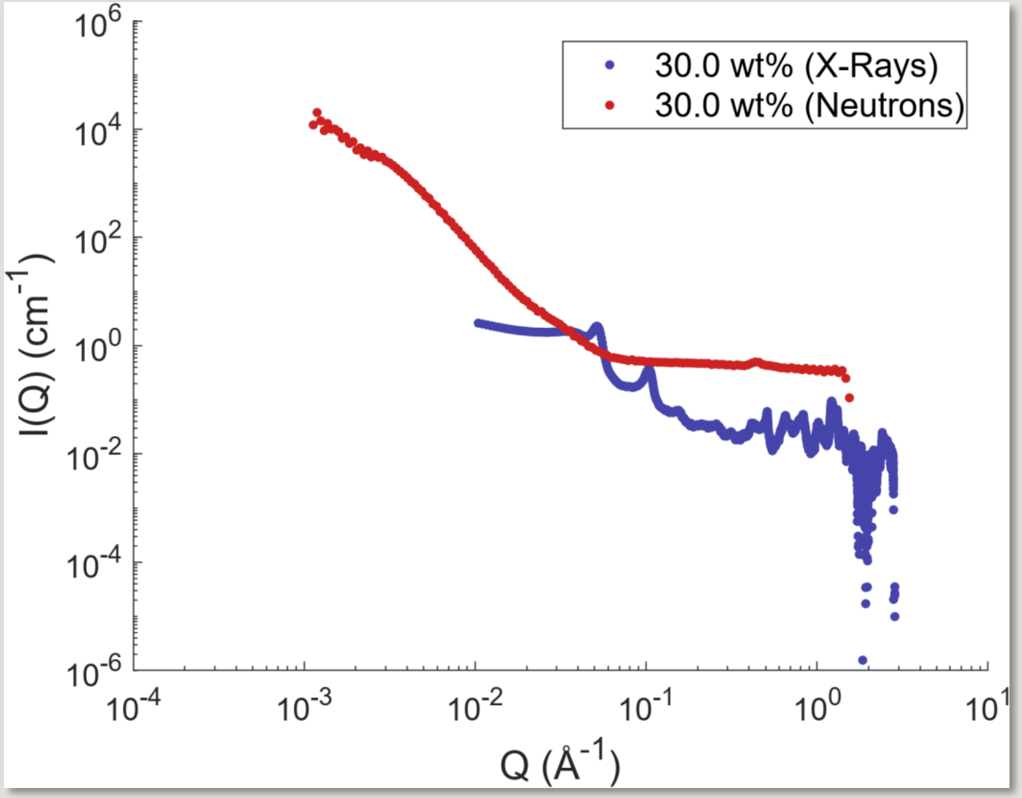

lamellar_stack_paracrystal Model Fitting – Raw Data

sample	concentration	background	error	scale	error	Nlayers	error	d_spacing	error	sigma_d	error	thickness	error	X^2
5A	7.5	3.6318E-06	2.8093E-02	3.9084E-01	1.1141E-03	3.8269E+00	4.4691E-02	2.4934E+02	1.4759E-01	6.2764E-02	3.2191E-03	2.6302E+00	2.8842E+01	8.9507
6A	10	1.7741E-07	3.0989E-03	7.6143E-01	2.4814E-03	5.4764E+00	5.9880E-02	2.2914E+02	8.2188E-02	6.3246E-02	5.1847E-04	1.4399E+01	5.4875E-01	18.652
7A	15	2.8180E-02	2.7798E-04	1.7703E+00	4.5201E-03	6.6491E+00	5.8205E-02	1.7909E+02	4.3471E-02	5.7677E-02	3.5589E-04	2.5379E+01	6.5646E-02	22.91
8A	20	2.5091E-02	3.7408E-04	2.0632E+00	5.6064E-03	1.0457E+01	1.5140E-01	1.5586E+02	3.6304E-02	6.2845E-02	3.5145E-04	2.4295E+01	7.0081E-02	42.746
9A	22.5	4.5582E-02	7.9176E-04	3.2838E+00	1.8328E-02	1.0569E+01	1.2259E-01	1.2689E+02	2.7204E-02	5.1189E-02	4.7271E-04	2.9457E+01	1.2023E-01	56.273
10A	25	3.0886E-02	7.6085E-04	3.8791E+00	1.7334E-02	9.5918E+00	1.5194E-01	1.2982E+02	3.5502E-02	1.7334E-02	4.4086E-04	2.9528E+01	1.0042E-01	25.784
11A	27.5	2.8919E-02	7.1873E-04	3.9127E+00	1.7799E-02	8.5022E+00	8.0421E-02	1.1546E+02	2.4681E-02	5.7803E-02	4.2741E-04	2.9367E+01	1.0050E-01	28.406
12B	30	3.9406E-02	3.9193E-04	2.2963E+00	1.0334E-02	8.4077E+00	8.8577E-02	1.1657E+02	2.8128E-02	5.9877E-02	5.2205E-04	3.0463E+01	9.7483E-02	18.874
13B	35	3.9630E-02	3.2523E-04	1.8982E+00	8.9735E-03	5.7868E+00	7.7784E-02	1.2298E+02	5.2324E-02	9.3762E-02	6.7624E-04	3.0820E+01	1.0243E-01	9.2532